ACS APPLIED MATERIALS & INTERFACES

www.acsami.org

Research Article

Understanding the "Anti-Catalyst" Effect with Added CoO_x Water Oxidation Catalyst in Dye-Sensitized Photoelectrolysis Cells: Carbon Impurities in Nanostructured SnO_2 Are the Culprit

Carly F. Jewell, Ashwanth Subramanian, Chang-Yong Nam,* and Richard G. Finke*

Cite This: *ACS Appl. Mater. Interfaces* 2022, 14, 25326–25336

Read Online

ACCESS | Metrics & More | Article Recommendations | Supporting Information

ABSTRACT: In 2017, we reported a dye-sensitized, photoelectrolysis cell consisting of fluorine-doped tin oxide (FTO)-coated glass covered by SnO_2 nanoparticles coated with *N*,*N*′-bis(phosphonomethyl)-3,4,9,10-perylenediimide (PMPDI) dye and then a photoelectrochemically deposited CoO_x water oxidation catalyst (WOCatalyst), FTO/nano-SnO_2/PMPDI/CoO_x. This system employed nanostructured SnO_2 stabilized by a polyethyleneglycol bisphenol A epichlorohydrin (PEG-BAE) copolymer and other C-containing additives based on a literature synthesis to achieve a higher surface area and thus greater PMPDI dye absorption and resultant light collection. Surprisingly, the addition of the well-established WOCatalyst CoO_x resulted in a *decrease* in the photocurrent, an unexpected *"anti-catalyst" effect*. Two primary questions addressed in the present study are (1) what is the source of this "anti-catalyst" effect? and (2) are the findings of broader interest? Reflection on the synthesis of nano-SnO_2 stabilized by PEG-BAE, and the large, ca. 10:1 ratio of C to Sn in synthesis, led to the hypothesis that even the annealing step at 450 °C in of the FTO/SnO_2 anode precursors was unlikely to remove all the carbon initially present. Indeed, residual carbon impurities are shown to be the culprit in the presently observed "anti-catalyst" effect. The implication and anticipated broader impact of the results of answering the two abovementioned questions are also presented and discussed along with a section entitled "Perspective and Suggestions for the Field Going Forward."

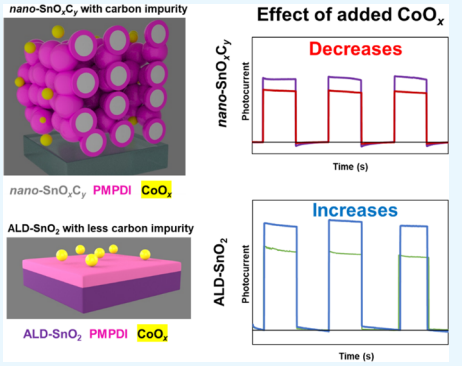

KEYWORDS: *dye-sensitized photoelectrochemical cell, perylene diimide, cobalt oxide, water oxidation catalysis, tin oxide, metal oxide, catalysis*

INTRODUCTION

Increasing global demand for energy has led to the declaration that water splitting into hydrogen and oxygen is one of the "Holy Grails" of Chemistry.[1−7] However, many of the best-performing water oxidation systems use precious rare-earth metals, limiting their commercial viability.[4,5,8,9] Ideally, the method used to achieve water splitting would involve *earth-abundant materials*.[8,10−13] In 2014, we published a then novel first-generation photoelectrochemical water oxidation catalysis (WOC) system consisting simply of the perylene diimide dye, *N*,*N*′-bis(phosphonomethyl)-3,4,9,10-perylenediimide (PMPDI) spin-coated onto indium tin oxide (ITO) plus a photoelectrochemically deposited CoO_x catalyst, denoted ITO/PMPDI/CoO_x, where anode notation here and in what follows is written in the order of deposition of the indicated components, ITO, PMPDI, and then CoO_x, as shown in Figure 1. This first-generation system provided modest photocurrents of ca. 150 μA/cm^2, but with a faradaic efficiency for O_2 of 80 ± 15% under +0.9 V bias versus Ag/AgCl.[14] However, this deliberately simple initial system was able to harvest only 12% of incident light at the dye's λ_{max}.[14] Highly relevant for what follows is that addition of CoO_x as a water oxidation catalyst (WOCatalyst) in this original planar system

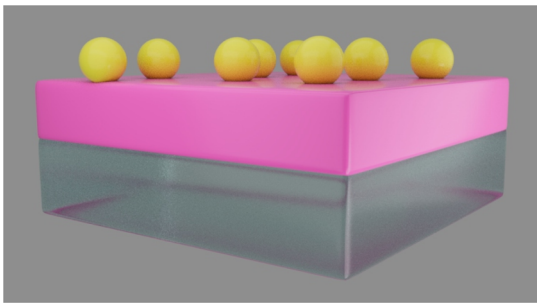

Figure 1. Idealized structural model of the ITO/PMPDI/CoO_x anode where ITO is clear, PMPDI is pink, and CoO_x is yellow. Anode notation throughout is written in the order of component deposition, left to right: ITO is used as a base layer, PMPDI is then deposited on the ITO, and then CoO_x is added atop the ITO/PMPDI.

Received: February 13, 2022
Accepted: May 2, 2022
Published: May 25, 2022

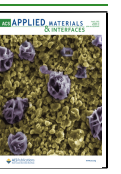

improved the photocurrent—that is, had the expected "positive catalyst effect" on water oxidation catalysis—in every ITO/PMPDI/CoO_x anode examined.[14]

To overcome the low light-harvesting by the planar system, as shown in Figure 1, a second-generation, high surface area, nanostructured system was constructed consisting of fluorine-doped tin oxide (FTO)-coated glass covered by SnO_2 nanoparticles coated with PMPDI dye and, then, photoelectrochemically deposited CoO_x WOCatalyst, FTO/SnO_2/PMPDI/CoO_x,[14,15] as shown in Figure 2. The higher surface

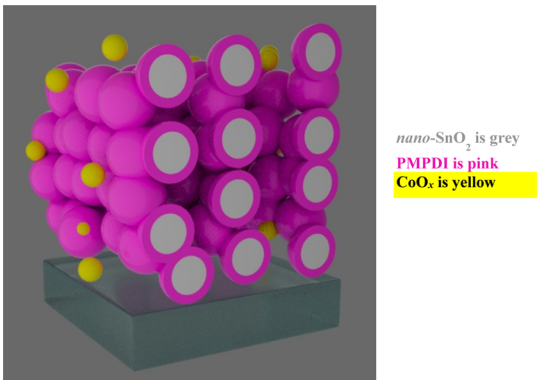

Figure 2. Idealized structural model of the FTO/nano-SnO_2/PMPDI/CoO_x anode where FTO is clear, SnO_2 is gray, PMPDI is pink, and CoO_x is yellow. For simplicity, only a small layer of the relatively much thicker, 18 μm, nano-SnO_2 is shown.

area afforded by the nanostructured SnO_2 worked as expected, allowing a higher dye loading, as shown visually in Figure 3, and a resultant >99% light-harvesting efficiency at the λ_{max} of the dye.[15]

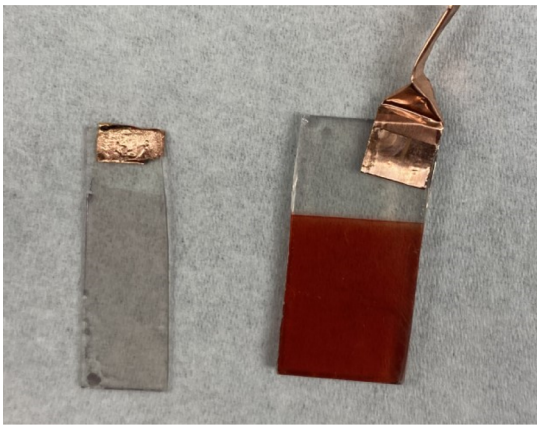

Figure 3. Image of the ITO/PMPDI/CoO_x anode (left) and FTO/nano-SnO_2/PMPDI/CoO_x anode (right), where only the bottom two thirds of each anode is dyed. The right-most FTO/SnO_2/PMPDI/CoO_x anode is obviously darker, clear visual evidence for the larger amount of dye present in the nanostructured, higher surface area, second-generation FTO/nano-SnO_2/PMPDI/CoO_x system.

However, an unexpected, undesired effect of adding the CoO_x WOCatalyst in the nano-SnO_2-based system is that it *lowers* the observed photocurrent, that is, added CoO_x results in an "anti-catalyst" effect in this second-generation device.[15] This "anti-catalyst" behavior was attributed to the increased charge recombination between photoinjected electrons in the SnO_2 conduction band and accumulated holes in CoO_x at the SnO_2 surface, that is, trap states at the CoO_x/SnO_2 interface.[15−17]

Highly relevant here is that others, too, have seen such an "anti-catalyst" effect, specifically Kamire et al. in their nano-TiO_2 sensitized by perylene monoimide dye using an Ir-dimer-based catalyst.[18] Such "anti-catalyst" effects in photoelectrochemical devices illustrate the acknowledged, broader challenge[13,19] of coupling catalysts to light-absorbing units in ways that minimize charge-carrier-recombination back reactions. Hence, an understanding of the origins and implications of the "anti-catalyst" effect is of fundamental interest and, we will learn, likely considerably broader implications.

Literature Syntheses of Polymer-Stabilized Nano-SnO_2. Nanostructured metal-oxide films, such as the one used herein for SnO_2 in Scheme 1, have been used in both dye-sensitized solar cells and dye-sensitized photoelectrolysis cells (DS-PECs), and as such, there are numerous preparations for such pastes and film formulations.[15,18,20−22] As detailed in Scheme 1, the nano-SnO_2 used in our second-generation DS-PEC was prepared using a commercial SnO_2 nanoparticle powder (NanoArc, Alpha Aesar) wetted with glacial acetic acid and water, then stabilized with the copolymer polyethyleneglycol bisphenol A epichlorohydrin (PEG-BAE) before one drop of Triton X-100 (octyl phenoxy polyethoxyethanol) is added for improved glass adhesion.[15,23] This nano-"SnO_2" is then doctor bladed onto conductive glass and annealed under air at 450 °C.

An attempt at a balanced stoichiometry for the literature nano-SnO_2 synthesis in so far as possible prior to the present work is shown in eq 1 in Scheme 1. The resultant value of 10:1 of added carbon to SnO_2 highlights the significant amount of carbon present in the nano-SnO_2 formulation. Equation 1 makes clear that crucial, but unknown, is the amount of carbon, "C_y," that remains present in the final product initially referred to as nano-"SnO_2" but hereafter denoted more precisely as nano-SnO_xC_y. Equation 2 also makes apparent how *un*atom-economical[24] and *un*green[25−27] the literature-based synthesis[15,23] of nano-SnO_2 is, in which 10 equiv of C are added when 0 equiv of C is desired in the resultant product!

A key for what follows is that the thermal annealing in air is implied in the literature, and arguably generally believed, to remove completely the polymer stabilizer and all other traces of carbon, ostensibly, as CO_2 shown in eq 1. Restated in other terms, in the present nano-SnO_xC_y is the y really zero as believed in the literature? If not, what, then, is the value of y? What actually is, then, nano-"SnO_2" in terms of nano-SnO_xC_y?

In considering possible origins for the "anti-catalyst" effect of adding the well-established CoO_x WOCatalyst,[14,15,28−31] it occurred to us that residual carbon not removed by even a 450 °C annealing under O_2 was a possible, if not probable, source of recombination sites in the system. The possibilities for the form(s) of residual carbon range from carbon black, to graphite, to graphene oxide, the later more oxidized form seemingly more reasonable given that the high-temperature annealing takes place under air. Of note here is the carbon removal as CO_2 likely leaves oxygen defects in the nano-SnO_xC_y system as well. The effects of such carbon states on the resulting kinetics[32,33] of the system are rarely taken into account. A kinetic scheme is presented later on as one illustrative, visual working hypothesis for the photoelectrochemical systems studied herein.

https://doi.org/10.1021/acsami.2c02692
ACS Appl. Mater. Interfaces 2022, 14, 25326−25336

Scheme 1. Equation 1 Shows the Literature Synthetic Procedure for Nano-SnO_xC_y Where First SnO_2, Acetic Acid, and Water are Added; Second, PEG-BAE is Added; Third, Triton X-100 is Added; Fourth, the Mixture is Heated to 450 °C in Air and Held at That Temperature for 1 h; This Results in Nano-SnO_xC_y As Well As Various Other Hypothesized Byproducts; Eq 2 is a Simplified Version of Eq 1, Where the Moles of SnO_2 are Set to 1 (i.e., by Dividing Eq 1 through by 0.0053), Thereby Highlighting the 10:1 Carbon to SnO_2 Precursor Ratio in Synthesis

Modified Literature-Based Synthesis[15,23]

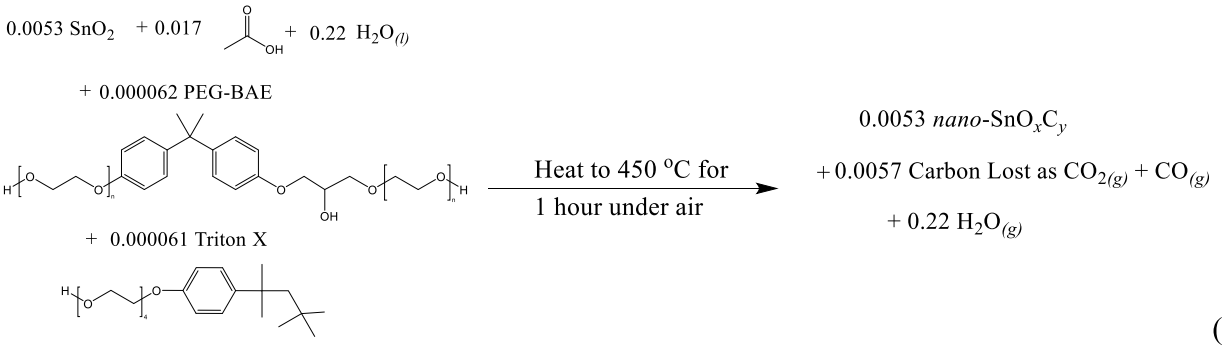

(1)

Simplified Stoichiometry for SnO_2 and C-Based Components

$$1\ SnO_2 + 10\ C \rightarrow 1\ SnO_xC_y + (10\text{-}y)\ C \quad (2)$$

Specific Questions Addressed in This Work and Their Significance. The specific questions addressed herein are the following: (1) first, is C left as an impurity in nano-"SnO_2"? (2) Second, if so, what then is y in "SnO_xC_y"? And third (3) if $y \neq 0$ so that C-impurities are present, then is that C-impurity in turn a source of enhanced recombination in the FTO/nano-SnO_2/PMPDI/CoO_x system? That is, are C-impurities directly connected to the observed "anti-catalyst effect" of added, otherwise effective, CoO_x WOCatalyst? Additionally, we will probe (4) if cleaner atomic layer deposition (ALD) of SnO_2 can be used to deposit lower-C SnO_2 in a, then, SnO_2-modified *planar* version of our WOC system, FTO/ALD-SnO_2/PMPDI/CoO_x? If so, does that low carbon system exhibit a normal "positive catalyst" effect?

Significance of the Present Studies. The significance of the present studies goes considerably beyond the current system given that many nano-metal-oxide syntheses found throughout the literature make use of such organic stabilizers/thickeners[15,22,31,34−37] or carbon-based starting materials.[32] The organic components of these nano-M_xO_y systems are often ignored as they are either thought to be removed fully through annealing,[15,38] or if observed, are not taken into consideration of the kinetics and efficiency of those systems.[32,33] Carbon impurities may in fact be common in nano-M_xO_y systems used in water oxidation catalysis. Additionally, oxygen, O-atom vacancies in WO_3 are known and have been studied in a FTO/nano-WO_3 system where oxygen-vacancy concentrations have been changed, and the authors then study which charge-transfer pathways are most favorable in that FTO/nano-WO_3 system.[32] Notably relevant for the present paper, that otherwise excellent, state-of-the-art system and study report the presence of carbon impurities (in both the text and as seen by X-ray photoelectron spectroscopy (XPS) in the accompanying Supporting Information section),[32] but then ignore those C-impurities. Those C-based impurities should have been, but were not, considered as an alternative explanation for the observed changes in charge separation and transport seen in the observed kinetics.[32]

Additionally, C-based impurities could be a part of the other literature system mentioned earlier that shows an "anti-catalyst" effect of added iridium dimer, a hypothesis that remains to be tested.[18] Overall, the results herein provide a recipe and associated working hypothesis for how to improve the catalyst efficiency in devices that employ metal-oxide nanoparticles involving polymer stabilizers in preparation of the photoelectrochemical device.

EXPERIMENTAL SECTION

Experimental conditions used herein are identical to those in our previously published work,[14,15,31] unless stated explicitly otherwise. However, key experimental details are provided below as necessary to ensure that the present manuscript is largely self-contained.

Materials. The following starting materials and solvents were used as received to generate buffer solutions: KOH (Fisher, Certified ACS grade, 98.5%, 1.5% water, 0.00028% Fe, and 0.0008% Ni); KH_2PO_4 (Fisher, Certified ACS Grade, 99.3%, 0.0005% Fe); hydroquinone (Aldrich, >99%); and NANOpure water (Barnstead NANOpure ultrapure water system, 18.0 MΩ). NANOpure water was used for all experiments.

Synthesis of Nano-"SnO_2" Following the Literature, Actually Nano-SnO_xC_y. SnO_2 nanoparticle paste was prepared, as shown in Scheme 1, using a modified literature procedure[23] previously worked out for the present system.[15] Using a plastic spatula, 800 mg of white commercial SnO_2 nanopowder (SnO_2, NanoArc, Alpha Aesar, Lot Analysis: 99.6% SnO_2, 47 m^2/g specific surface area by BET, 18 nm average particle size, and 6.95 g/cm^3 density) was massed into a 20 mL scintillation vial. A Teflon-coated magnetic stir bar and 1.0 mL of glacial acetic acid (ACS grade, Mallinckrodt) were added, and the solution was mixed until all the SnO_2 powder was wet; this resulted in the formation of a gray paste. The vial containing this paste was then placed in an ultrasonic water bath (Branson 2510) for 5 min. Water, 4.0 mL, was added, and the solution was mixed on a stir plate. This paste was then sonicated twice using a QSonica Q125 ultrasonic liquid microprocessor (1/8″ probe, held at 80% amplitude) for 5 min to form a light gray suspension. Then, 1.10 g of PEG-BAE (Sigma, M_w = 15,000−20,000), which serves as a thickening agent, was added in individual small chunks while stirring over the course of an hour (S1 for reaction equation). New pieces were added only after complete dissolution of the previous addition, by visual inspection, to avoid clumping. Once all the PEG-BAE had been added and dissolved

https://doi.org/10.1021/acsami.2c02692
ACS Appl. Mater. Interfaces 2022, 14, 25326−25336

fully, one drop (approximately 20 mg) of Triton X-100 (octyl phenoxy polyethoxyethanol, Sigma) was added with a plastic transfer pipet to increase the adhesion of the paste to the glass substrate. This paste was stirred overnight and then refrigerated in a sealed vial for use over several days with no visual change. Before use, the paste was stirred for approximately 1 h and allowed to reach room temperature.

Planar SnO_2 Preparation by ALD. Ultrathin conformal coatings of SnO_x were prepared using the Cambridge Nanotech Savannah S100 ALD system (base pressure of ~0.43 Torr). The deposition temperature was set at 85 °C. The depositions were carried out by sequential exposures to tetrakis(dimethylamido)tin(IV) (TDMASn) (Strem Chemicals) (200 ms) and water vapor (15 ms) with an intermediate purge time of 10 s for both the precursors. To calibrate the thickness of SnO_2 deposited, the deposition cycles were initially chosen as 25, 50, 75, and 100. Spectroscopic ellipsometry was used to calibrate the SnO_x thickness per ALD cycle using Si control substrates and found a linear growth rate of 0.152 nm per cycle (Figure S1 and Table S1). The number of ALD cycles varied between 4 and 122 to deposit SnO_x with thickness ranging from 0.6 to 18.0 nm as desired.

Synthesis of PMPDI dye, and the Deposition of SnO_2 Anode and CoO_x WOCatalyst. All synthetic and manufacturing details for PMPDI dye can be found in our previous publications.[14,15] Briefly, the anodes are composed of FTO-coated glass as a transparent current collector, covered by SnO_2, either a mesoporous nano-"SnO_2" or SnO_2 by ALD. The SnO_2-coated anodes were then sensitized with PMPDI, and CoO_x was photoelectrochemically deposited as the water oxidation catalyst. All fabricated photoanodes have SnO_2 films with "2-Scotch" layer thickness conditions[15] where PMPDI dyes were loaded for 24 h at 95 °C from a saturated solution of fully protonated PMPDI in water.[15] CoO_x WOCatalyst was added to photoanodes by photoelectrochemical deposition.[14,15] The anodes (SnO_2/PMPDI) were submerged in a solution of pH 7, 0.5 mM $Co(NO_3)_2$ and 0.1 M potassium phosphate butter (KPi) and held at +0.2 V versus Ag/AgCl under 1 sun illumination for 3 min.[15] Anodes were then rinsed with water for 30 s and allowed to air dry.

Photoelectrochemical Testing. All photoelectrochemical experiments were carried out in a previously described[15,31] custom two-compartment Pyrex cell consisting of a working compartment (1 × 1.5 × 1.5 cm^3, 5 mL) and an auxiliary compartment separated by a medium porosity glass frit. Experiments were conducted using a CH Instruments CHI-750D bipotentiostat, a Pt wire counter electrode, and a Ag/AgCl (3 M NaCl, +0.215 V vs normal hydrogen electrode) reference electrode. The reference electrode was positioned in the working compartment in close proximity to the anode surface, and the counter electrode was placed in the auxiliary compartment. The anode was clamped with an alligator clip to the front wall of the working compartment with the nonconductive glass side pressed flush to the cell wall. Then, both compartments of the cell were filled with ca. 5 mL electrolyte (pH 7, 0.1 M KPi buffer), sufficient to cover the film. The anode was illuminated from the substrate side using a 65 W xenon arc lamp (PTO model A1010), which was powered using an OLIS XL150 adjustable power supply. The light passed through a bandpass filter (315−710 nm, Thorlabs KG3, FGS900S) and an ultraviolet (UV) filter (400 nm long-pass, Thorlabs FGL400S) before reaching the anode. The power density of the light was adjusted to reflect the visible region of the airmass 1.5 global (AM 1.5G) spectrum.[15] In the experiments in which transients (interrupted illumination) were used, a manual shutter was used to block the light.[15] Each anode was tested with a series of electrochemical experiments in the order detailed below. First the cell was allowed to short-circuit in the dark for 60 s to depopulate the electrons from SnO_2 sub-band gap states.[15] Then, the open-circuit potential, V_{oc}, was measured versus the Ag/AgCl reference electrode for 90 s in the dark and then again under illumination. Next, a photocurrent transient experiment was performed, in which the anode was held at +0.2 V versus Ag/AgCl for 300 s with 30 s light/dark transients throughout. The anode was then allowed to short-circuit in the dark for 60 s, and the V_{oc} in both the dark and light was remeasured. Then, the current−voltage (i−V) photocurrent transient experiment was performed. The voltage was scanned from −0.2 to +1.0 V versus Ag/AgCl with a 10 mV/s scan rate and 5 s light transients. Each experiment was reproduced a minimum of three times with three separate, independent anodes produced under identical conditions. All figures and values reported herein are representative of the photoactivity of the system indicated. Care was taken to ensure that the reported results are reproducible and not due to a defective anode or otherwise irreproducible sample.

Thermogravimetric Analysis. Thermogravimetric analysis (TGA) was carried out using a TA Instruments TGA 2950 thermogravimetric analyzer under air flow. The heating regime used mimicked the above nano-"SnO_2" synthesis exactly; the temperature was ramped from 20 to 450 °C, ramping 20 °C/min, and held for 1 h. A platinum TGA pan was used to hold the sample.

X-ray Photoelectron Spectroscopy. XPS was carried out using a PE-5800 series Multi-Technique ESCA XPS system where a Al Kα monochromatic source operating at 350.0 W was used for all XPS experiments. High-resolution (HRES) scans were carried out for all elements present in the initial survey scan at a minimum of three spots across the sample surface for 30 min apiece. To fit the data, CASAXPS software was used to analyze the data. Quantification results for each element were tabulated using an average of each replicate scan. Consistent with both the literature method of XPS fitting and ensuring the self-consistency across fits, HRES spectra were calibrated to a 285 eV aliphatic carbon peak.[39,40] Sputtering was carried out using Ar^+ ions at 5 kV for 1 min over a 3 × 3 mm^2 area. The area analyzed by XPS was taken from the center of the sputtered region.

Scanning Electron Microscopy. Scanning electron microscopy (SEM) images were taken for nano-"SnO_2"/PMPDI and ALD-SnO_2 anodes using a JEOL JSM-6500F field emission scanning electron microscope, using 15 kV accelerating voltage and 10 mm working distance. Energy-dispersive X-ray spectrometry (SEM−EDS) data were collected using an Oxford Instruments energy-dispersive X-ray spectrometer. Qualitative and quantitative elemental analyses were carried out using Oxford Aztec software. A nano-"SnO_2"/PMPDI anode was cracked in half and was then coated in 10 nm of gold to examine the cross section. Of note, the sample had to be oriented at a slight angle off of vertical.

Oxygen Detection. Oxygen yield was experimentally measured using the generator−collector (G−C) technique detailed elsewhere.[15,41−43] Briefly, photoanode "generators" were sandwiched with an FTO "collector,"[15] separated by a Parafilm spacer. The resultant G−C cell was placed in the previously detailed working compartment with the generator side flush to the wall of the cell nearest the incoming light. The cell was filled with pH 7, 0.1 M KPi buffer, approximately 10 mL, which was degassed with Ar for a minimum of 60 min. Current was measured at both the generator and collector electrodes, which were held at +0.2 and −0.65 V versus Ag/AgCl, respectively. The current was collected for 300 s in the dark, 300 s in the light, then 300 s in the dark to ensure all oxygen diffused across the two electrodes, and current attributable to oxygen production was detected. Control experiments with FTO/CoO_x anodes were used to determine the collection efficiency of the sandwich configuration[15] and used to calculate the O_2 yield and Faradaic efficiency of each photoanode.

RESULTS AND DISCUSSION

In-House Nano-"SnO_2" Synthesis and Carbon Impurities. As detailed in the Experimental Section, current nano-"SnO_2" synthesis (really nano-SnO_xC_y synthesis, vide infra) relies heavily on a large excess of organic stabilizers, resulting in a final paste with a formulation of ca. 11 wt % SnO_2, 15 wt % acetic acid, 17 wt % PEG-BAE, and 57 wt % water,[15] Scheme 1, vide supra. As Scheme 1 points out, this results in a hugely atom-uneconomical ~10:1 molar ratio of C-to-SnO_2 in the initial paste—10 moles of C-impurity versus 1 mole of the desired SnO_2. To attempt to remove the carbon, once the paste is deposited on the conductive glass, the literature

https://doi.org/10.1021/acsami.2c02692
ACS Appl. Mater. Interfaces 2022, 14, 25326−25336

synthesis sinters the anodes under air in a furnace, in which the temperature is gradually increased (ca. 20 °C/min) to 450 °C; the temperature is then held at 450 °C for an hour before very gradual (less than 1 °C/s) cooling back to room temperature. During this carbon-removal sintering process (i.e., attempted full removal of the PEG-BAE, Triton X-100, and acetic acid), a carbon-free, pure nano-"SnO_2" has been thought to be formed.[44] However, the specific literature hypothesis that y = 0 for the SnO_xC_y product has not been quantitatively tested until now.

Post some reflection, we hypothesized that carbon impurities remain in the nano-"SnO_2" prepared by the literature route[15,23] and that this residual carbon is what is causing the observed, decreased water oxidation performance, and the "anti-catalyst" effect.[15] As a test of this hypothesis and the specific question of "is y in SnO_xC_y in fact ≠ 0?," an initial control experiment of a TGA on just the PEG-BAE organic stabilizer was run, in which the TGA conditions were set to mimic the 450 °C in the air annealing method used on the anodes, Figure 4. After the full

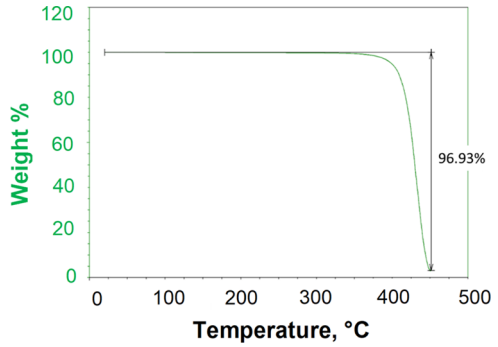

Figure 4. Figure: TGA of 17.56 mg of PEG-BAE stabilizer placed in a platinum TGA pan. Ramped from 20 to 450 °C, ramping 20 °C/min, and held 1 h. This procedure mimics the typical sintering conditions used on the nano-SnO_xC_y for anode production. After 1 h at 450 °C 3.1% of the PEG-BAE, 0.54 mg, remained, indicating that all the C present initially is *not* removed by this thermal treatment.

TGA schedule of 450 °C for 1 h, *3.1% of the PEG-BAE remained*, indicating that not all the carbon is removed during at least this particular sintering process on a platinum TGA pan, resulting visually in a black powder as expected for elemental C. Residual carbon in a, then, FTO/nano-SnO_xC_y/PMPDI/CoO_x photoelectrochemical device is particularly concerning as the CoO_x catalyst deposition is accomplished photoelectrochemically, implying that the expected high electrical conductivity of residual carbon could play a significant role in the placement and properties of the CoO_x WOCatalyst.

A second control experiment was carried out in which, now, the *nano-SnO_xC_y paste* was sintered at 450 °C for varying amounts of time: unsintered (0 h), sintered traditionally for 1 h, and sintered for *7 days*. Each of these pastes were then examined using XPS, Table 1 and Supporting Information Section S3. The unsintered paste had the expected significant amount of carbon, ca. 66%. In both samples sintered for either 1 h or 7 days, a greater amount of carbon remained, approximately 11%, in the nano-SnO_xC_y film for both the samples regardless of the 1 h versus 7 days of sintering. Noteworthy is that sintering the nano-SnO_xC_y paste for even 7 days does not remove more C within experimental error in comparison to the traditional 1 h at 450 °C. No matter how long we sinter at 450 °C, a significant amount of carbon, roughly 11% C, remains in the sample. Of note here is that the difference between 69 and 11% (or at most ∼15% from the last entry in Table 1) is far greater than any error due to adventitious carbon[45] in the experiment.

Table 1. XPS Characterization of Sintered Nano-SnO_xC_y under Several Conditions

XPS of nano-SnO_xC_y	unsintered (0 h)[a]	sintered 1 h[a]	sintered for 7 days[a]
weight percent C	65.5 ± 5.0	11.1 ± 0.3	13.6 ± 1.3

[a]Three independent anodes, analyzed at three spots on each anode.

As a control, a more bulk-sensitive (i.e., less-surface-sensitive) technique, SEM−EDS, was also used to verify the amount of carbon in the normal, 1 h sintered sample (i.e., in an attempt to decouple any potential adventitious surface-adsorbed carbon, a part of most XPS samples, from the amount of carbon remaining in the sintered nano-SnO_xC_y). Specifically, SEM−EDS was carried out on the cross section of a deliberately cracked nano-SnO_xC_y anode, Figure 5a,b. *There is clearly carbon present throughout the cracked anode*, indicating that there is incorporation of the carbon throughout the nano-SnO_xC_y, and indicating that the majority of the ∼11% C in the standard 1 h sintered samples is not from any source of adventitious carbon. Moreover, a clear distinction in the amount of carbon present can be seen where the FTO glass is, indicating that the carbon in the bulk nano-SnO_xC_y sample is well beyond the background of any/all types of adventitious carbon. Moreover, by EDS, the carbon was found to be 10.8 ± 0.8 wt % in sections of the nano-SnO_xC_y anode, quantitatively comparable to the 11.1 ± 0.3 wt % of carbon by XPS. The EDS and XPS results in turn yield y = 0.22, that is, nano-"SnO_2" is really nano-$SnO_xC_{0.22}$. Noteworthy here is that the ∼11% residual carbon in the nano-SnO_xC_y is higher than the 3.1% residual carbon in the TGA experiment on just the PEG-BAE stabilizer, consistent with the expectation that carbon in SnO_xC_y should be—and experimentally is—harder to remove.

Hence, our first three specific questions have been answered: (1) yes, C is left as an impurity in nano-"SnO_2," that is, $y \neq 0$ in "SnO_xC_y"; (2) y = 0.22, or ∼11 wt %, even in the XPS control of 7 days of 450 °C sintering in air of nano-SnO_xC_y; (3) yes, a viable hypothesis is, then, that residual C is likely influencing the charge-transfer kinetics of the FTO/nano-$SnO_xC_{0.22}$/PMPDI/CoO_x photoelectrochemical WOC system, for example, as carbon-defect-based trap states. It follows that the nano-$SnO_xC_{0.22}$-based system needs to be further examined to see whether it exhibits the observed, "anti-catalyst" effect post adding the well-established, normally "positive" WOCatalyst, CoO_x.

Testing the Carbon Impurity Hypothesis by Changing the Carbon Level. To probe the leading hypothesis that carbon impurities in the nano-$SnO_xC_{0.22}$ are the source of the "anti-catalyst" inefficiency in our nanostructured, nano-$SnO_xC_{0.22}$-based anodes, anodes with differing amounts of carbon present were prepared and then tested. In order to best replicate the (precisely unknown) form(s) of carbon present in the nano-SnO_xC_y, the amount of PEG-BAE organic stabilizer used in the synthesis was altered. Specifically, using an otherwise identical synthesis, anodes with half as much PEG-BAE and, then, twice as much PEG-BAE added into the SnO_2 paste as the traditional synthesis were fabricated and tested (denoted as 0.5 equiv PEG-BAE anodes and 2 equiv PEG-BAE

https://doi.org/10.1021/acsami.2c02692
ACS Appl. Mater. Interfaces 2022, 14, 25326−25336

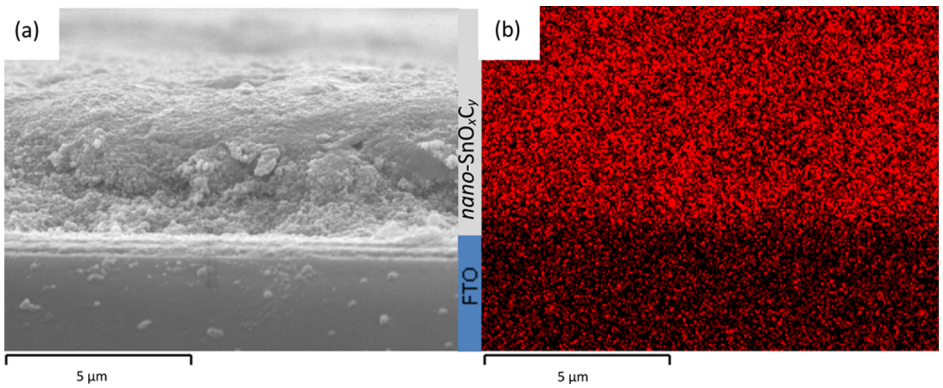

Figure 5. (a) SEM image of a nano-SnO_xC_y anode taken at 30,000× magnification. Image is a profile of the cross section of the anode after deliberately cracking. The FTO glass is clearly visible at the bottom of the SEM image of the cross section for reference and perspective. (b) EDS image of the same anode in the same orientation showing only the distribution of carbon across the sample in red. For clarity at the left of (b) (i.e., in between the (a,b)), a bar labeling the areas of the cross section is included between the two figures where the blue represents the FTO conducting glass, and the light gray is the nano-SnO_xC_y.

anodes, respectively). Importantly, SEM−EDS characterization of the carbon in the 0.5 equiv PEG-BAE anodes and for the 2 equiv PEG-BAE anodes verified the synthetic strategy by showing 7.8 ± 0.8 and 26.7 ± 0.7 wt %, respectively (Figure S3), in the respective anodes.

In each case, the addition of the CoO_x catalyst once again resulted in a decrease in the steady-state photocurrent for all the used PEG-BAE amounts (Figure 6a). Significantly, the experimentally observed photocurrent decrease *correlates directly with the amount of carbon*, added initially as PEG-BAE, in the nano-SnO_xC_y: the anodes with only 0.5 equiv of PEG-BAE exhibit a *smaller decrease* in photocurrent with the addition of the catalyst, 22 ± 4%, while the anodes with 2 equiv PEG-BAE have a *larger decrease* in photocurrent, 58 ± 3%. These data constitute arguably prima facie evidence for a direct connection between the amount of carbon impurity present in the nano-SnO_xC_y and the degree of "anti-catalyst" behavior following the addition of the CoO_x WOCatalyst.

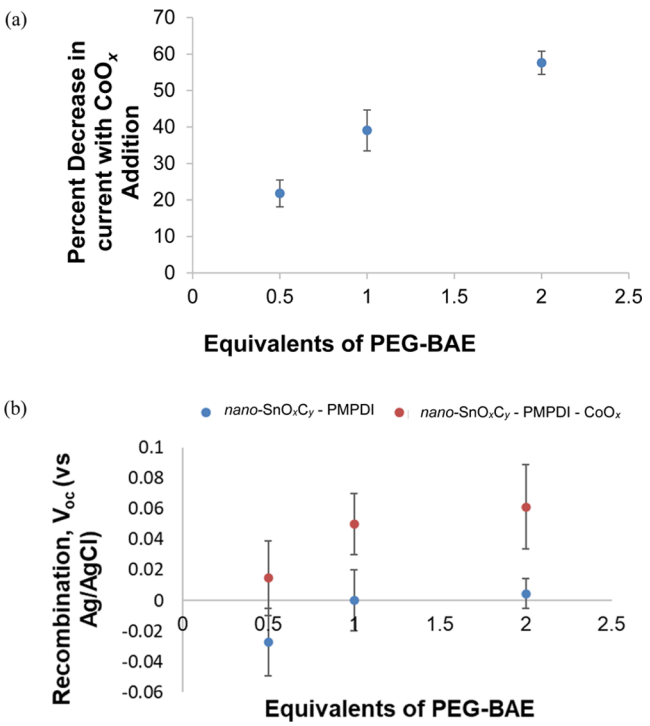

Figure 6. (a) Percent loss of steady-state photocurrent with the addition of the CoO_x catalyst at differing amounts of PEG-BAE addition where 1 equiv is the amount added in a typical, traditional synthesis. (b) V_{oc} vs Ag/AgCl reference electrode in a half-cell setup for nano-SnO_xC_y/PMPDI (blue) and nano-SnO_xC_y/PMPDI CoO_x (red) anodes at differing amounts of PEG-BAE addition where 1 equiv is the amount added in a typical, traditional synthesis. In this case, $V_{oc} \approx E_{F,n}$, the quasi-Fermi energy of electrons in the SnO_2 sub-band gap states.[15,31]

Also noteworthy here *is the fact that each anode, regardless of amount of PEG-BAE added, was found to have the same concentration of dye within experimental error by UV−visible spectroscopy* (Figure S4 in Supporting Information). As such, those data rule out the otherwise plausible alterative hypothesis that the "anti-catalyst" effect is due to differing degrees of *overall binding* between the PMPDI dye and the metal-oxide surface[36] (still due, in this alternative hypothesis, to the presence of carbon). However, note here that we cannot say that different dye morphologies or some other different structural parameter does not result in the FTO/nano-$SnO_xC_{0.22}$/PMPDI/CoO_x system due to the carbon impurity. Indeed, a rational probe of the mechanism(s) behind the effect(s) of carbon impurities requires first and at a minimum the synthesis and characterization of a presently unknown, pure nano-"SnO_2." Hence, deeper insights into the role(s) of carbon impurities will have to be the focus of needed future efforts and studies. The main message of the present work is "avoid carbon impurities" until and unless you are sure you want them in your particular system.

Open-Circuit Potential Data, V_{oc}. To better understand the role of the carbon impurity in FTO/nano-SnO_xC_y/PMPDI/CoO_x systems, recombination was studied. To estimate the relative amount of recombination, the open-circuit potential (V_{oc}) of the anode under illumination was measured for anodes prepared from different starting amounts of PEG-BAE and, hence, differing amounts of carbon, *y*, in the nano-SnO_xC_y (Figure 6b).[15,31,46] V_{oc} values reflect the quasi-Fermi energy of electrons ($E_{F,n}$) in the nano-SnO_xC_y substrate with respect to a Ag/AgCl reference electrode potential.[15,31,46] Steady-state charge-carrier concentration determines the V_{oc}, meaning the relative rates at which electrons are injected from the photoexcited dye to SnO_2 versus the rate of depopulation

https://doi.org/10.1021/acsami.2c02692
ACS Appl. Mater. Interfaces 2022, 14, 25326−25336

of the SnO_2 via recombination set that in/out equilibrium. Experimentally, in anodes with half as much PEG-BAE, *no significant increase in recombination was observed with the addition of catalysts*, Figure 6b. However, in anodes prepared under normal, 1 equiv, PEG-BAE addition and with 2 equiv of PEG-BAE, *an increase in recombination with the deposition of CoO_x catalyst occurs*, Figure 6b. With higher, 1 equiv amounts of PEG-BAE leading to higher levels of C-impurities, there is also an increase in recombination compared to anodes with less PEG-BAE, Figure 6b.

The V_{oc} data in Figure 6a,b provide strong, if not compelling, evidence that the carbon impurity from the organic stabilizer in the resultant nano-SnO_xC_y plays a key role in determining the recombination kinetics. Altering the concentration of the C-impurity significantly shifts the relative ratios of at least some kinetic pathways within the charge-carrier kinetics. The origins of the "anti-catalyst" effect are thereby traced to the presence of C-impurity. The evidence is compelling that if carbon impurities are present, then their role(s) in the charge-carrier kinetics of the system must be included in at least the present system and, by implication, in the future discussions of DS-PEC systems more generally. The fact that the C-impurity comes from an *un*atom-economical[24] and *un*green[25−27] literature synthesis, that starts out with a 10:1 C to SnO_2 ratio in a synthesis that is aimed at a 0:1 ratio of C to SnO_2 in the product, makes apparent the future goal of designing syntheses of nanostructured M_xO_y stabilized by a minimum of presumably non-polymeric, ideally readily removable stabilizing ligands. Just such studies aimed at purer nano-SnO_2 are in progress.

Testing the Effect of Added C-Black. As one additional test of the effects of deliberately added carbon, anodes were produced with the direct addition of carbon black as a well-known, specific type of carbon. Recombination was found to significantly increase with the inclusion of carbon black at both two and five equiv of added carbon black (Figure S6 of Supporting Information). Hence, these experiments with added C-black provide additional evidence for and verification of the data and conclusions from the above, varied PEG-BAE equivalents, study. Additionally, as in anodes in which carbon black is added, the same trends are observed as in anodes with PEG-BAE addition, data that argue any changes in the oxygen concentration that may arise with PEG-BAE variation is not a dominant effect in this system. In total, the results presented herein provide strong support for the hypothesis that carbon impurities lead to enhanced recombination in at least the present FTO/SnO_xC_y/PMPDI/CoO_x WOC system and almost surely in other, related systems as well.

Kinetics Scheme for the FTO/SnO_xC_y/PMPDI/CoO_x System as a Working Hypothesis Going Forward. In order to better visualize the impacts of carbon impurities on the charge-transfer pathways throughout the system, a kinetics scheme for the SnO_xC_y/PMPDI/CoO_x system was constructed as a working hypothesis for going forward, Scheme 2.

Kinetic pathways are identified using k_{trans}, $k_{scavenge}$, k_{inj}, k_{recomb}, k_{abs}, k_{bet}, and k_{relax}, indicating, respectively, electron transfer, scavenging, injection, recombination, absorbance, back electron transfer, and relaxation. Inherent charge-recombination pathway rate constants are shown in red, whereas the new pathways due to C-based recombination are shown in blue. For simplicity, the carbon impurities are depicted as a single state, although realistically multiple different potentials at points where the carbon impurities sit

Scheme 2. Hypothetical Kinetics Scheme of the SnO_xC_y/PMPDI/CoO_x System Intended as an Illustrative Working Hypothesis[a]

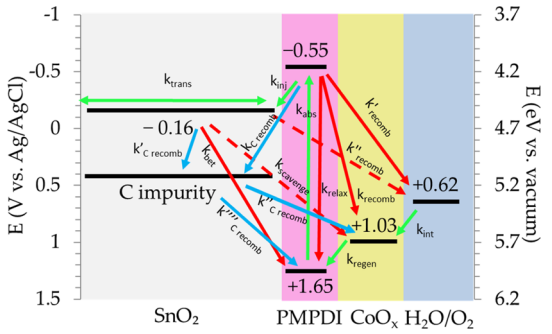

[a]SnO_2 is white, PMPDI is pink, and CoO_x is yellow. The blue arrows indicate possible recombination pathways from any carbon defects present in "SnO_xC_y," whereas green arrows indicate idealized pathways for charge transfer in the water oxidation catalysis. Red arrows indicate loss of efficiency in the form of charge-carrier recombination. All other potential impurities and defects, including O-vacancy defects,[32] are omitted from this scheme for the sake of simplicity, but oxygen-defects are also possible and might even impact carbon-based recombination.

are likely, approaching a band of potentials for carbon impurity and a "dispersive kinetics" type of situation.[47,48] The addition of charge-transfer pathways, particularly recombination, involving carbon impurities shows the numerous pathways, in which carbon impurities can alter the charge-transfer kinetics. Simply omitting the blue arrows from Scheme 2 provides an illustration of a hypothetical system free of impurities and defects. Future fast spectroscopic kinetics study and data will be needed to provide evidence for or against the specific pathways postulated in Scheme 2 and their relative rate constants.

Further Test of the C-Impurities and Thereby Enhanced Recombination Hypothesis: Photocurrents from SnO_2 Films by ALD in the System. A prediction from the "C-impurities cause enhanced recombination" hypothesis and from the kinetics shown in Scheme 2 is that the addition of a lower C-content SnO_2 layer *in the planar system* might be able to overcome the "anti-catalyst" effect and might even exhibit a positive effect upon the addition of CoO_x. ALD can provide films with a low defect density and is a deposition method able to produce a better controlled system with fewer impurities.[49−52] Hence, SnO_2 deposition by ALD was employed to generate what proved to be the desirable lowered-carbon form of SnO_2.[53]

Specifically, ALD-deposited SnO_2 was added in a planar layer to yield FTO/ALD-SnO_2/PMPDI, as detailed in the Experimental Section. Although anodes for WOC testing used 5 nm thick layers of ALD-SnO_2, a much thicker, 18 nm, layer of ALD-SnO_2 was deposited and utilized to examine the amount of carbon impurity (i.e., with the goal of emphasizing carbon in the bulk material and not surface-adsorbed adventitious carbon). SEM−EDS examination of this FTO/ALD-SnO_2 yielded 1.68 ± 0.02 wt % carbon. The surface of the SnO_2 deposited by ALD showed 5 ± 3% carbon by XPS, while mild sputtering to remove adventitious carbon from normal room air and vacuum grease[45] showed ca. 3 ± 3% carbon by XPS. Hence, there is significantly less carbon in the

https://doi.org/10.1021/acsami.2c02692
ACS Appl. Mater. Interfaces 2022, 14, 25326−25336

ALD-SnO_2 than that in the nano-SnO_xC_y both by XPS and SEM−EDS.

The photoelectrochemical performance of the FTO/ALD-SnO_2(5 nm)/PMPDI anodes, using 5 nm thick layers of ALD-SnO_2, was studied in pH 7 buffer. As the SnO_2 deposited by ALD is planar, the electrochemically active surface area is much smaller than that for the three-dimensional nano-SnO_xC_y, and, as such, the expected photocurrents are lower than that in the nano-SnO_xC_y-based system. Hence, hydroquinone (H_2Q) was examined as before[14,15] as a sacrificial reductant that undergoes a kinetically facile, $2e^-$ and $2H^+$ oxidation (i.e., one closer to the $4e^-$ and $4H^+$ required for water oxidation[4,15,54] and, therefore, a better model for water oxidation catalysis than common, sacrificial reductants such as $K_4Fe^{II}(CN)_6$[14,55,56] and its $1e^-$, $Fe^{II/III}$ redox couple). Photocurrent transients were carried out on ALD-SnO_2 anodes with and without catalysts in the presence of H_2Q (Figure 7).

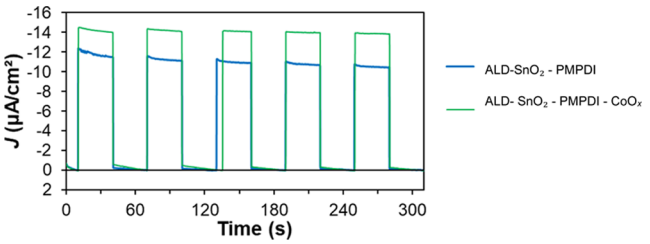

Figure 7. *J*−*t* transients in the presence of 20 mM H_2Q sacrificial reductant, with background dark current subtracted, at +0.2 V vs Ag/AgCl in pH 7, 0.1 M KPi buffer with 30 s light/dark transients where blue is FTO/ALD-SnO_2(5 nm)/PMPDI and green is FTO/ALD-SnO_2(5 nm)/PMPDI/CoO_x.

Significantly, the observed photocurrents *increased* ca. 31% with the addition of CoO_x, as shown in Figure 6, from ca. −10.5 to −13.8 $\mu A/cm^2$, indicating that CoO_x deposition onto the ALD-SnO_2 coated with dye yields the desired *positive effect* of adding the CoO_x WOCatalyst. In short, reducing the carbon impurity even further, as low as currently feasible using ALD-SnO_2 in the planar FTO/ALD-SnO_2(5 nm)/PMPDI/CoO_x system, is able to overcome the "anti-catalyst effect." These results therefore confirm and compliment those seen with the nano-SnO_xC_y system. Overall, the results to this point provide strong support for carbon impurities as the culprit in enhancing recombination in the nanostructured FTO/SnO_xC_y/PMPDI/CoO_x system.

Nano-SnO_xC_y/ALD-SnO_2/PMPDI. In an attempt to find a sort of goldilocks version of the SnO_2 systems, in which the increased surface area and hence enhanced dye absorbance of the nano-SnO_xC_y was somehow balanced by the decreased carbon impurities of ALD-SnO_2, a "double SnO_2" system combining both forms of SnO_2 was tested. Specifically, anodes consisting of nano-SnO_xC_y were coated with a relatively thick, 18 nm of ALD-SnO_2, with dye and then CoO_x catalyst was deposited. This thick, 18 nm, layer of SnO_2 was chosen as a compromise to coat at least a significant part of the nano-SnO_xC_y without the loss of too much of the higher surface area provided by the nano-SnO_xC_y. Again, the amount of dye on the nano-SnO_xC_y/ALD-SnO_2/PMPDI was found to be comparable to that of the nano-SnO_xC_y/PMPDI anodes by UV−vis, suggesting that PMPDI binds to the SnO_2 with a similar affinity on the nano-SnO_xC_y/PMPDI and on the thin, non-nanostructured, ALD-SnO_2 (Figure S4 of Supporting Information).

The resultant photocurrent transient data showed, however, that even with an 18 nm coating of ALD-SnO_2, the addition of the catalyst *still decreases the photoactivity* (Figure S8 of Supporting Information), that is, still shows the "anti-catalyst" effect post adding CoO_x. While it is conceivable that an even thicker ALD-SnO_2 layer *might* work better, the results suggest that, instead, future research efforts would be better placed toward developing superior, *carbon-free syntheses of SnO_2 and other M_xO_y nanoparticles.* As already noted, such needed efforts are in progress.

Demonstration of Water Oxidation Catalysis by the ALD-SnO_2/PMPDI/CoO_x Anodes. Actual water oxidation for the ALD-SnO_2/PMPDI/CoO_x anodes, which were found to display improved photocurrents with catalyst addition in hydroquinone (Figure 7), vide supra, was measured in the absence of any sacrificial reagent as a control to ensure that the photocurrent observed in the hydroquinone system is representative of the anode's WOC properties (Figure 8).

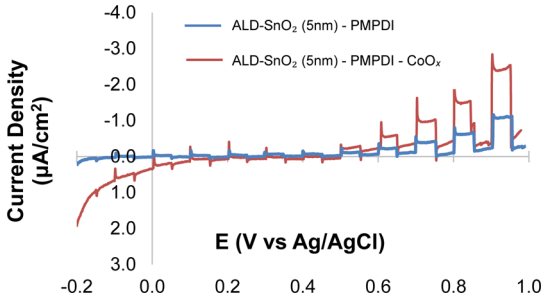

Figure 8. Photocurrent transients for ALD-SnO_2(5 nm)/PMPDI (blue) and ALD-SnO_2(5 nm)/PMPDI/CoO_x (red), anodes. Scans were carried out from −0.2 to +1.0 V vs Ag/AgCl with 5 s light dark transients. Note background currents and current from background FTO subtracted off.

Importantly, the addition of CoO_x catalysts showed a positive water-oxidation catalysis response, improving the photocurrent. Although challenging due to the expected low, $\mu A/cm^2$ range, photocurrents for the planar system, Faradaic efficiencies for water oxidation catalysis could be calculated and hence were also measured for the ALD-SnO_2/PMPDI/CoO_x system using the generator-collector method.[15,43] The observed Faradaic efficiencies were found to be 45 ± 6%, an improvement over the 31 ± 7% for the nano-SnO_xC_y/PMPDI/CoO_x system.[15] The observed improvement in photocurrent with the addition of catalyst in actual WOC for the ALD-SnO_2 system is, once more, consistent with and supportive of the carbon impurity hypothesis.

The ALD-SnO_2 systems have a higher (more positive) photocurrent-onset-potential, and a larger overpotential is required to see significant amounts of photocurrent. This change in needed overpotential is interesting and implies altered kinetics of charge transfer between the two systems with their differing types of SnO_2 and nanostructured versus planar morphologies. The significant spiking behavior, seen previously and attributed to charge recombination caused by metal-oxide surface states, is still present.[15,16,57−59]

Perspective and Suggestions for the Field Going Forward. Historically, the impact that carbon-based impurities in metal oxides have on charge-transfer kinetics in DS-

https://doi.org/10.1021/acsami.2c02692
ACS Appl. Mater. Interfaces 2022, 14, 25326−25336

PECs is a neglected area of study or, even, recognition. The role of C-based impurities is typically dismissed or at least insufficiently examined. Herein, we have demonstrated that residual-carbon impurities play a significant part in determining the effectiveness of charge transfer for water oxidation in the system examined, and likely in many other metal-oxide systems that make use of especially polymeric carbon-based stabilizers that are difficult or nearly impossible to subsequently remove completely. Our findings teach that the role of impurities, carbon-based as discussed herein, oxide-based as discussed elsewhere,[32] and likely other-element impurities specific to a given system, must be included in the discussion of kinetics and other explanations of the system at hand and its properties.

Additionally, creating at least a working kinetic scheme such as Scheme 2 is important en route to understanding complex photocatalytic systems, such as WOC systems, and the interconnected pathways that dictate net charge transfer. More specifically, C-based impurities as a now precedented hypothesis for recombination need to be considered in systems with metal-oxide nanoparticles involving polymeric or other hard-to-remove (if not impossible to remove completely) stabilizers. The broader applicability of our results is illustrated by their relevance to a state-of-the art 2020 system[32] where oxide impurities are considered, but carbon impurities are noted but not assessed. *Both* carbon impurities and oxide defects need to be addressed in such cases as both can play critical roles in altering the kinetics of charge-transfer pathways and, hence, the overall WOC results.

It is important here to note that advanced techniques like ALD that involve much less carbon are certainly more costly and technically involved than the simple doctor blading method used for nano-SnO_xC_y. Such more sophisticated methods are less easily scalable and, hence, may not be sustainable, long-term solutions to depositing metal-oxides with lowered carbon content. As such, our results highlight strongly the need to develop M_xO_y nanoparticle syntheses without the use of polymer stabilizers and, if possible, readily and completely removable meta-stabilizers. Indeed, this need reflects a more general theme and need throughout nanoparticle chemistry, one we have addressed in $M(0)_n$ (M = transition-metal) nanoparticles via the concept of "weakly ligated, labile ligand" nanoparticles.[60] Such improved syntheses should also strive to be closer to being atom economical[24] and to obeying the relevant principles of green chemistry.[25−27] Alternative syntheses of pure nano-"SnO_2," as well as other metal-oxides, that balance minimizing carbon impurity while maximizing surface area are, hence, of considerable interest.[61] Notable here is the Boettcher group's development of precursor chemistry for the deposition of both undoped and F-doped SnO_2 films; using minimal nonfunctional counterions, no organic ligands, and water as a solvent is a promising pathway toward realizing the development of SnO_2 without detrimental carbon states.[61] Perhaps another approach to overcome the recombination kinetics inherent in a material with carbon impurity is the addition of a more efficient catalyst, conceivably one derived from less earth-abundant metals. This approach is under investigation as well.

CONCLUSIONS

Herein, we examined WOC systems consisting of SnO_2, both nano-"SnO_2" that proved to actually be SnO_xC_y and planar SnO_2 deposited by ALD, coated with PMPDI with a CoO_x catalyst. We were able to answer four important questions: (1) first, is C left as an impurity in nano-"SnO_2"? *Answer: yes.* (2) Second, if so, what then is y in "SnO_xC_y"? *Answer:* $y = 0.22$. Third (3) if $y \neq 0$ so that C-impurities are present, then is that C-impurity in turn a source of enhanced recombination in the FTO/nano-SnO_xC_y/PMPDI/CoO_x system. That is, are C-impurities primarily responsible for the observed "anti-catalyst effect" of added, normally effective CoO_x WOCatalyst? *Answer: yes.* (4) Can cleaner ALD deposition of SnO_2 be used to deposit lower-C SnO_2 in a, then, planar SnO_2-modified version of our WOC system, FTO/ALD-SnO_2/PMPDI/CoO_x. If so, does the resulting system exhibit a normal "positive catalyst" effect? *Answer: yes.* Finally, a short section on "Perspective and Suggestions for the Field Going Forward" was provided with the goal of more efficient future research involving M_xO_y nanoparticles in photoelectrochemical devices without the pitfalls that C-based impurities otherwise engender.

ASSOCIATED CONTENT

Supporting Information

The Supporting Information is available free of charge at https://pubs.acs.org/doi/10.1021/acsami.2c02692.

Details on carbon black addition to nano-SnO_xC_y paste, information on how the balanced chemical reaction for the preparation of nano-SnO_xC_y was determined, and further information on the ALD of SnO_2 (PDF)

AUTHOR INFORMATION

Corresponding Authors

Chang-Yong Nam − *Center for Functional Nanomaterials, Brookhaven National Laboratory, New York, New York 11973, United States; Department of Materials Science and Chemical Engineering, Stony Brook University, Stony Brook, New York 11794, United States;* orcid.org/0000-0002-9093-4063; Email: cynam@bnl.gov

Richard G. Finke − *Department of Chemistry, Colorado State University, Fort Collins, Colorado 80523, United States;* orcid.org/0000-0002-3668-7903; Email: richard.finke@colostate.edu

Authors

Carly F. Jewell − *Department of Chemistry, Colorado State University, Fort Collins, Colorado 80523, United States;* orcid.org/0000-0003-3177-3690

Ashwanth Subramanian − *Department of Materials Science and Chemical Engineering, Stony Brook University, Stony Brook, New York 11794, United States;* orcid.org/0000-0003-1400-1533

Complete contact information is available at: https://pubs.acs.org/10.1021/acsami.2c02692

Notes

The authors declare no competing financial interest.

ACKNOWLEDGMENTS

This research was supported by the National Science Foundation under grant no. 1664646. The authors thank the members of Prof. Finke's research group and Dr. Christopher Whitehead for reading draft versions of this manuscript and providing valuable feedback. Thanks also to the Analytical Research Core at Colorado State University for instrument access and assistance and Audrey Jewell for the production of

artistic renderings. This research used the Materials Synthesis and Characterization Facility of the Center for Functional Nanomaterials, which is a U.S. DOE Office of Science Facility, at Brookhaven National Laboratory under contract no. DE-SC0012704.

REFERENCES

(1) Lewis, N. S.; Nocera, D. G. Powering the Planet: Chemical Challenges in Solar Energy Utilization. *Proc. Natl. Acad. Sci. U.S.A.* **2006**, *103*, 15729−15735.
(2) Smalley, R. E. Future Global Energy Prosperity: The Terawatt Challenge. *MRS Bull.* **2005**, *30*, 412−417.
(3) Kudo, A.; Miseki, Y. Heterogeneous Photocatalyst Materials for Water Splitting. *Chem. Soc. Rev.* **2009**, *38*, 253−278.
(4) Kirner, J. T.; Finke, R. G. Water-Oxidation Photoanodes Using Organic Light- Harvesting Materials: A Review. *J. Mater. Chem. A* **2017**, *5*, 19560−19592.
(5) Tachibana, Y.; Vayssieres, L.; Durrant, J. R. Artificial Photosynthesis for Solar Water-Splitting. *Nat. Photonics* **2012**, *6*, 511−518.
(6) Swierk, J. R.; Mallouk, T. E. Design and Development of Photoanodes for Water-Splitting Dye-Sensitized Photoelectrochemical Cells. *Chem. Soc. Rev.* **2013**, *42*, 2357−2387.
(7) Roger, I.; Shipman, M. A.; Symes, M. D. Earth-Abundant Catalysts for Electrochemical and Photoelectrochemical Water Splitting. *Nat. Rev. Chem.* **2017**, *1*, 0003.
(8) Kärkäs, M. D.; Verho, O.; Johnston, E. V.; Rn Åkermark, B. Artificial Photosynthesis: Molecular Systems for Catalytic Water Oxidation. *Chem. Rev.* **2014**, *114*, 11863−12001.
(9) Ye, S.; Ding, C.; Liu, M.; Wang, A.; Huang, Q.; Li, C. Water Oxidation Catalysts for Artificial Photosynthesis. *Adv. Mater.* **2019**, *31*, 1902069.
(10) Kondo, M.; Tatewaki, H.; Masaoka, S. Design of Molecular Water Oxidation Catalysts with Earth-Abundant Metal Ions. *Chem. Soc. Rev.* **2021**, *50*, 6790−6831.
(11) Kondo, M.; Masaoka, S. Water Oxidation Catalysts Constructed by Biorelevant First-Row Metal Complexes. *Chem. Lett.* **2016**, *45*, 1220−1231.
(12) Du, P.; Eisenberg, R. Catalysts Made of Earth-Abundant Elements (Co, Ni, Fe) for Water Splitting: Recent Progress and Future Challenges. *Energy Environ. Sci.* **2012**, *5*, 6012−6021.
(13) Singh, A.; Spiccia, L. Water Oxidation Catalysts Based on Abundant 1st Row Transition Metals. *Coord. Chem. Rev.* **2013**, *257*, 2607−2622.
(14) Kirner, J. T.; Stracke, J. J.; Gregg, B. A.; Finke, R. G. Visible-Light-Assisted Photoelectrochemical Water Oxidation by Thin Films of a Phosphonate-Functionalized Perylene Diimide Plus CoO_x Cocatalyst. *ACS Appl. Mater. Interfaces* **2014**, *6*, 13367−13377.
(15) Kirner, J. T.; Finke, R. G. Sensitization of Nanocrystalline Metal Oxides with a Phosphonate- Functionalized Perylene Diimide for Photoelectrochemical Water Oxidation with a CoO_x Catalyst. *ACS Appl. Mater. Interfaces* **2017**, *9*, 27625−27637.
(16) Prasittichai, C.; Hupp, J. T. Surface Modification of SnO_2 Photoelectrodes in Dye-Sensitized Solar Cells: Significant Improvements in Photovoltage via Al_2O_3 Atomic Layer Deposition. *J. Phys. Chem. Lett.* **2010**, *1*, 1611−1615.
(17) Swierk, J. R.; McCool, N. S.; Saunders, T. P.; Barber, G. D.; Mallouk, T. E. Effects of Electron Trapping and Protonation on the Efficiency of Water-Splitting Dye-Sensitized Solar Cells. *J. Am. Chem. Soc.* **2014**, *136*, 10974−10982.
(18) Kamire, R. J.; Materna, K. L.; Hoffeditz, W. L.; Phelan, B. T.; Thomsen, J. M.; Farha, O. K.; Hupp, J. T.; Brudvig, G. W.; Wasielewski, M. R. Photodriven Oxidation of Surface-Bound Iridium-Based Molecular Water-Oxidation Catalysts on Perylene-3,4-Dicarboximide-Sensitized TiO_2 Electrodes Protected by an Al_2O_3 Layer. *J. Phys. Chem. C* **2017**, *121*, 3752−3764.
(19) National Science Foundation. *Catalytic Chemistry Workshop on Defining Critical Directions for the Future*, 2011; pp 1−20.
(20) Zhu, K.; Neale, N. R.; Miedaner, A.; Frank, A. J. Enhanced Charge-Collection Efficiencies and Light Scattering in Dye-Sensitized Solar Cells Using Oriented TiO_2 Nanotubes Arrays. *Nano Lett.* **2006**, *7*, 69−74.
(21) Adachi, M.; Murata, Y.; Takao, J.; Jiu, J.; Sakamoto, M.; Wang, F. Highly Efficient Dye-Sensitized Solar Cells with a Titania Thin-Film Electrode Composed of a Network Structure of Single-Crystal-like TiO_2 Nanowires Made by the "Oriented Attachment" Mechanism. *J. Am. Chem. Soc.* **2004**, *126*, 14943−14949.
(22) Wang, D.; Xu, Z.; Sheridan, M. V.; Concepcion, J. J.; Li, F.; Lian, T.; Meyer, T. J. Photodriven Water Oxidation Initiated by a Surface Bound Chromophore-Donor-Catalyst Assembly. *Chem. Sci.* **2021**, *12*, 14441−14450.
(23) Brennan, B. J.; Durrell, A. C.; Koepf, M.; Crabtree, R. H.; Brudvig, G. W. Towards Multielectron Photocatalysis: A Porphyrin Array for Lateral Hole Transfer and Capture on a Metal Oxide Surface. *Phys. Chem. Chem. Phys.* **2015**, *17*, 12728−12734.
(24) Trost, B. M. The Atom Economy-A Search for Synthetic Efficiency. *Science* **1991**, *254*, 1471−1477.
(25) Anastas, P. T.; Williamson, T. C. *Green Chemistry: Designing Chemistry for the Environment*; American Chemical Series Books; American Chemical Society: Washington, DC, 1996; pp 1−20.
(26) Anastas, P.; Eghbali, N. Green Chemistry: Principles and Practice. *Chem. Soc. Rev.* **2010**, *39*, 301−312.
(27) Anastas, P. T.; Warner, J. C. *Green Chemistry: Theory and Practice*; Oxford University Press: New York, 1998.
(28) Kanan, M. W.; Nocera, D. G. In Situ Formation of an Oxygen-Evolving Catalyst in Neutral Water Containing Phosphate and Co^{2+}. *Science* **2008**, *321*, 1072−1075.
(29) Du, P.; Kokhan, O.; Chapman, K. W.; Chupas, P. J.; Tiede, D. M. Elucidating the Domain Structure of the Cobalt Oxide Water Splitting Catalyst by X-Ray Pair Distribution Function Analysis. *J. Am. Chem. Soc.* **2012**, *134*, 11096−11099.
(30) Kanan, M. W.; Surendranath, Y.; Nocera, D. G. Cobalt-phosphate oxygen-evolving compound. *Chem. Soc. Rev.* **2009**, *38*, 109−114.
(31) Jewell, C. F.; Subramanian, A.; Nam, C.-Y.; Finke, R. G. Ultrathin alumina passivation for improved photoelectrochemical water oxidation catalysis of tin oxide sensitized by a phosphonate-functionalized perylene diimide first without, and then with, CoO_y. *Sustain. Energy Fuels* **2021**, *5*, 5257−5269.
(32) Corby, S.; Francàs, L.; Kafizas, A.; Durrant, J. R. Determining the Role of Oxygen Vacancies in the Photoelectrocatalytic Performance of WO_3 for Water Oxidation. *Chem. Sci.* **2020**, *11*, 2907−2914.
(33) Santato, C.; Odziemkowski, M.; Ulmann, M.; Augustynski, J. Crystallographically Oriented Mesoporous WO_3 Films: Synthesis, Characterization, and Applications. *J. Am. Chem. Soc.* **2001**, *123*, 10639−10649.
(34) Ronconi, F.; Syrgiannis, Z.; Bonasera, A.; Prato, M.; Argazzi, R.; Caramori, S.; Cristino, V.; Bignozzi, C. A. Modification of Nanocrystalline WO_3 with a Dicationic Perylene Bisimide: Applications to Molecular Level Solar Water Splitting. *J. Am. Chem. Soc.* **2015**, *137*, 4630−4633.
(35) Meda, L.; Tozzola, G.; Tacca, A.; Marra, G.; Caramori, S.; Cristino, V.; Alberto Bignozzi, C. Photo-Electrochemical Properties of Nanostructured WO3 Prepared with Different Organic Dispersing Agents. *Sol. Energy Mater. Sol. Cells* **2010**, *94*, 788−796.
(36) Bergeron, B. V.; Marton, A.; Oskam, G.; Meyer, G. J. Dye-Sensitized SnO_2 Electrodes with Iodide and Pseudohalide Redox Mediators. *J. Phys. Chem. B* **2005**, *109*, 937−943.
(37) Lindquist, R. J.; Phelan, B. T.; Reynal, A.; Margulies, E. A.; Shoer, L. E.; Durrant, J. R.; Wasielewski, M. R. Strongly Oxidizing Perylene-3,4-Dicarboximides for Use in Water Oxidation Photoelectrochemical Cells. *J. Mater. Chem. A* **2016**, *4*, 2880−2893.
(38) Palomares, E.; Clifford, J. N.; Haque, S. A.; Lutz, T.; Durrant, J. R. Slow Charge Recombination in Dye-Sensitised Solar Cells (DSSC) Using Al_2O_3 Coated Nanoporous TiO_2 Films. *Chem. Commun.* **2002**, *14*, 1464−1465.

https://doi.org/10.1021/acsami.2c02692
ACS Appl. Mater. Interfaces 2022, 14, 25326−25336

(39) Evans, S. Correction for the Effects of Adventitious Carbon Overlayers in Quantitative XPS Analysis. *Surf. Interface Anal.* **1997**, *25*, 924−930.
(40) Greczynski, G.; Hultman, L. X-Ray Photoelectron Spectroscopy: Towards Reliable Binding Energy Referencing. *Prog. Mater. Sci.* **2020**, *107*, 100591.
(41) Zhao, Y.; Swierk, J. R.; Megiatto, J. D., Jr.; Sherman, B.; Youngblood, W. J.; Qin, D.; Lentz, D. M.; Moore, A. L.; Moore, T. A.; Gust, D.; Mallouk, T. E. Improving the Efficiency of Water Splitting in Dye-Sensitized Solar Cells by Using a Biomimetic Electron Transfer Mediator. *Proc. Natl. Acad. Sci. U.S.A.* **2012**, *109*, 15612−15616.
(42) Ashford, D. L.; Sherman, B. D.; Binstead, R. A.; Templeton, J. L.; Meyer, T. J. Electro-Assembly of a Chromophore-Catalyst Bilayer for Water Oxidation and Photocatalytic Water Splitting. *Angew. Chem., Int. Ed.* **2015**, *54*, 4778−4781.
(43) Sherman, B. D.; Sheridan, M. V.; Dares, C. J.; Meyer, T. J. Two Electrode Collector−Generator Method for the Detection of Electrochemically or Photoelectrochemically Produced O_2. *Anal. Chem.* **2016**, *88*, 7076−7082.
(44) Bagheri-Mohagheghi, M.-M.; Shahtahmasebi, N.; Alinejad, M. R.; Youssefi, A.; Shokooh-Saremi, M. The Effect of the Post-Annealing Temperature on the Nano-Structure and Energy Band Gap of SnO_2 Semiconducting Oxide Nano-Particles Synthesized by Polymerizing-Complexing Sol-Gel Method. *Phys. B* **2008**, *403*, 2431−2437.
(45) Barr, T. L.; Seal, S. Nature of the Use of Adventitious Carbon as a Binding Energy Standard. *J. Vac. Sci. Technol., A* **1995**, *13*, 1239−1246.
(46) Ardo, S.; Meyer, G. J. Photodriven Heterogeneous Charge Transfer with Transition-Metal Compounds Anchored to TiO_2 Semiconductor Surfaces. *Chem. Soc. Rev.* **2009**, *38*, 115−164.
(47) Plonka, A. Dispersive kinetics. *Annu. Rep. Prog. Chem., Sect. C: Phys. Chem.* **2001**, *97*, 91−147.
(48) Siebrand, W.; Wildman, T. A. Dispersive Kinetics: A Structural Approach to Nonexponential Processes in Disordered Media. *Acc. Chem. Res.* **1986**, *19*, 238−243.
(49) Kim, H. Y.; Nam, J. H.; George, S. M.; Park, J.-S.; Park, B. K.; Kim, G. H.; Jeon, D. J.; Chung, T.-M.; Han, J. H. Phase-Controlled SnO_2 and SnO Growth by Atomic Layer Deposition Using Bis(N-Ethoxy-2,2-Dimethyl Propanamido)Tin Precursor. *Ceram. Int.* **2019**, *45*, 5124−5132.
(50) Sundqvist, J.; Lu, J.; Ottosson, M.; Hårsta, A. Growth of SnO_2 Thin Films by Atomic Layer Deposition and Chemical Vapour Deposition: A Comparative Study. *Thin Solid Films* **2006**, *514*, 63−68.
(51) Mullings, M. N.; Hägglund, C.; Bent, S. F. Tin Oxide Atomic Layer Deposition from Tetrakis(Dimethylamino)Tin and Water. *J. Vac. Sci. Technol., A* **2013**, *31*, 061503.
(52) Heo, J.; Hock, A. S.; Gordon, R. G. Low Temperature Atomic Layer Deposition of Tin Oxide. *Chem. Mater.* **2010**, *22*, 4964−4973.
(53) Cheng, H.-E.; Tian, D.-C.; Huang, K.-C. Properties of SnO_2 Films Grown by Atomic Layer Deposition. *Procedia Eng.* **2012**, *36*, 510−515.
(54) Wee, K.-R.; Sherman, B. D.; Brennaman, M. K.; Sheridan, M. V.; Nayak, A.; Alibabaei, L.; Meyer, T. J. An Aqueous, Organic Dye Derivatized SnO_2/TiO_2 Core/Shell Photoanode. *J. Mater. Chem. A* **2016**, *4*, 2969−2975.
(55) McHugh, P. J.; Stergiou, A. D.; Symes, M. D. Decoupled Electrochemical Water Splitting: From Fundamentals to Applications. *Adv. Energy Mater.* **2020**, *10*, 2002453.
(56) Qureshi, M.; Shinagawa, T.; Tsiapis, N.; Takanabe, K. Exclusive Hydrogen Generation by Electrocatalysts Coated with an Amorphous Chromium-Based Layer Achieving Efficient Overall Water Splitting. *ACS Sustain. Chem. Eng.* **2017**, *5*, 8079−8088.
(57) Vandermolen, J.; Gomes, W. P.; Cardon, F. Closure to "Discussion of 'Investigation on the Kinetics of Electroreduction Processes at Dark TiO_2 and $SrTiO_3$ Single Crystal Semiconductor Electrodes' [J. Vandermolen, W. P. Gomes, and F. Cardon (pp. 324−328, Vol. 127, No. 2)]". *J. Electrochem. Soc.* **1980**, *127*, 2651.
(58) Salvador, P.; Gutiérrez, C. Mechanisms of Charge Transfer at the Semiconductor-Electrolyte Interface: I . Kinetics of Electroreduction at Dark of and in Aqueous Solution on a Sintered Nb-doped Electrode: Influence of pH. *J. Electrochem. Soc.* **1984**, *131*, 326−336.
(59) Ondersma, J. W.; Hamann, T. W. Measurements and Modeling of Recombination from Nanoparticle TiO_2 Electrodes. *J. Am. Chem. Soc.* **2011**, *133*, 8264−8271.
(60) Mondloch, J. E.; Özkar, S.; Finke, R. G. Weakly Ligated, Labile Ligand" Nanoparticles: The Case of $Ir(0)_n \cdot (H^+ Cl^-)$M. *ACS Omega* **2018**, *3*, 14538−14550.
(61) Nadarajah, A.; Carnes, M. E.; Kast, M. G.; Johnson, D. W.; Boettcher, S. W. Aqueous Solution Processing of F-Doped SnO_2 Transparent Conducting Oxide Films Using a Reactive Tin(II) Hydroxide Nitrate Nanoscale Cluster. *Chem. Mater.* **2013**, *25*, 4080−4087.

https://doi.org/10.1021/acsami.2c02692
ACS Appl. Mater. Interfaces 2022, 14, 25326−25336